

## X-Ray Diffraction Analyses of Titanium Dioxide Nanoparticles

M. Iniya Pratheepa<sup>1</sup>, M. Lawrence<sup>1\*</sup>

<sup>1</sup>Department of Physics, St. Joseph's College, Trichy-620 002, Tamilnadu, India

E-mail: jefflara1968@yahoo.co.in, Contact Number: +91- 9842459119, Trichy- 620 002, Tamilnadu, India

### Abstract

Titanium dioxide (TiO<sub>2</sub>) nanopowder was synthesized by cost effective hydrothermal method. The sample was subjected to X-ray diffraction analysis (XRD) and the average crystallite size was estimated from Debye Scherrer's formula and was found to be 30nm. XRD pattern measures the micro strain, bond length, volume, and dislocation density. The instrumental broadening analysis reveals the size and micro strain by Williamson-Hall Plot method. The result revealed that the morphology index is interrelated with particle size and specific surface area.

**Keywords:** XRD, Particle Size, Morphology Index, Specific Surface Area

### Introduction

TiO<sub>2</sub> is a most popular material with a large scale production. Several articles are reporting that anatase, brookite, and rutile are the most common phases. Each and every crystalline structure attributes particular physical properties, band gap, surface morphology and so on [1,2]. With the most noteworthy refractive index, rutile phase is used in artworks, paintings and inks [3]. The Catalysis and photo catalysis applications were effective in anatase nanoparticles [4-6]. It is additionally considered as the best contender for photovoltaic and electro chromic devices [7]. Brookite has not been used in the commercial product, but rather a dye sensitized solar cell as of recently reported with empowering out comes [8]. An essential effect on the surface properties of particle size was investigated and

reported by a number of researchers [9-11]. It is for the most part used as a photo-catalyst material on account of its lesser monetary value and chemical stability. It owns many applications in several industries like aerospace, medicine, paint, and cosmetics.

The present work is a report on synthesis of TiO<sub>2</sub> nanoparticles by cost effective co precipitation method. The synthesized material was investigated by X-Ray diffraction (XRD) analysis. Particle size, Microstrain, Dislocation density, Morphology index and specific surface area were estimated from the powder x-ray diffraction data.

### Experimental

#### Synthesis of TiO<sub>2</sub> nanoparticles

TiO<sub>2</sub> nanoparticles have been synthesized by hydrothermal method using 10 ml of titanium tetra isopropoxide (TTIP) in a mixture of 50 ml ethanol and 50 ml double distilled water. All procedures of synthesis of TiO<sub>2</sub> nanoparticles were proclaimed in this literature [12]. The final gel was dried at 80°C for 4 hour. Finally, a white powder was conflagrated at 500°C and the activities of TiO<sub>2</sub> samples were investigated.

The synthesized TiO<sub>2</sub> nanoparticles were subjected to powder X-Ray diffraction analysis using JEOL JDX Powder X-Ray diffractometer equipped with Cu-K $\alpha$  radiation of wavelength ( $\lambda$ )=1.5406 Å and the data were taken within the range of 10° to 70° with the step scan of 0.04.

### Results and Discussion

The XRD pattern Figure 1 affirms the presence of TiO<sub>2</sub> nanoparticles. The prominent peaks were compared with JCPDS data (PDF No: 21-1272) and the peaks obtained in the pattern coincides well with the literature. The intensity of the peak is high and the width of (101) plane at 2θ=25.313° becomes narrow [13]. The sharpness of the peak uncovers that the samples possess a good crystalline nature. The strong diffraction peak around 25.313° and 48.089° indicates TiO<sub>2</sub> is in anatase phase [14]. The spacious diffraction peak is not found in the pattern.

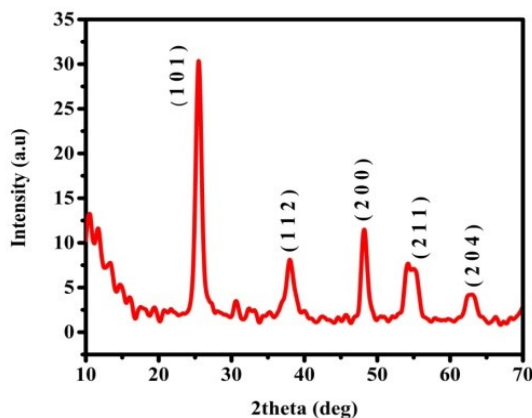


**Figure 1.** XRD Pattern of TiO<sub>2</sub> Nanoparticles

### Particle Size

Average crystallite size of TiO<sub>2</sub> was estimated from the Scherrer's equation as follows [20]

$$D = \frac{K\lambda}{\beta \cos \theta}$$

where, D is the crystallite size, K is the Scherer constant (0.89), λ is the X-ray wavelength (1.54 nm), β the peak width of half maximum, and θ is the Bragg diffraction angle. From the XRD result, grain sizes were calculated by X-Ray line broadening method using Scherrer equation and the plots were drawn with 1/β on X-axis and cosθ along the Y-axis as shown in Figure 2. By fitting the data, crystalline size (D) was extracted from the slope.

### Instrumental Broadening

At a point when the particle size is under 100 nm, appreciable broadening will occur in x-ray diffraction pattern because of particle size and strain. The average particles size is evaluated by the observed peak broadening. The total broadening of the diffraction peak is because of the material and instrument. The sample broadening is calculated by

$$FW(S) \times \cos = \frac{K\lambda}{\text{size}} + 4 \times \text{strain} \times \sin \theta$$

The total broadening βt equation is described by

$$\beta t^2 \approx \left( \frac{0.9\lambda}{D \cos \theta} \right)^2 + (4\varepsilon \tan \theta)^2 + \beta_0^2$$

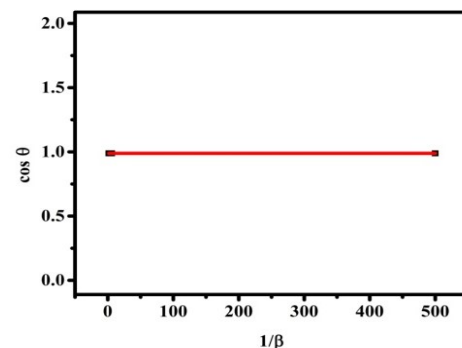


**Figure 2.** Scherrer Equation Plot of TiO<sub>2</sub> Nanoparticles

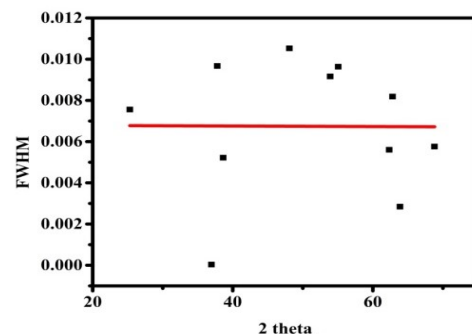


**Figure 3.** Typical Instrumental Broadening of TiO<sub>2</sub> nanoparticles

where D is average particle size, ε is strain and β<sub>0</sub> is instrumental broadening. The size and strain were experimentally observed. The broadening of several peaks was estimated using least squares method and presented in Figure 3. When, particle size becomes smaller, due to size effect, the peaks become broad

and widths larger. The broadening of peak may likewise happen because of micro strains of the crystal structure emerging from defects like dislocation and twinning [16].

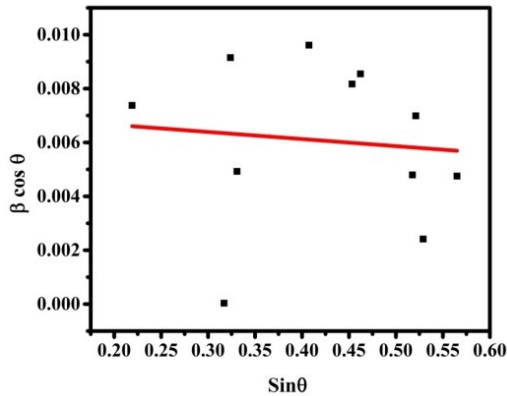


**Figure 4.** Williamson Hall Plot - TiO<sub>2</sub> Nanoparticles

Williamson and Hall proposed a method for deconvoluting size and strain broadening by looking at the peak width as a function of  $2\theta$  which is called as W-H method. The graph plotted is known as W-H plot and it is shown in Figure 4. It is plotted with  $\sin \theta$  on the x-axis and  $\beta \cos \theta$  on the y-axis (in radians). A linear fit gives the y-intercept and slope of which the particle size and strain are estimated respectively.

#### XRD - Specific Surface Area

Specific surface area (SSA) is a material property. It is an inferred scientific value that can be utilized to determine the type and properties of a material. It has a specific significance if there should arise an occurrence of adsorption, heterogeneous catalysis and responses on surfaces.

$$SSA = \frac{SA_{part}}{V_{part} \times D_{density}}$$

where SSA is the SA per mass, SSA & S are the specific surface area,  $V_{part}$  is particle volume and

$SA_{part}$  is Surface Area of particle and density of TiO<sub>2</sub> (4.23 g.cm<sup>-3</sup>).

$$S = \frac{6 \times 10^3}{D_p \times \rho}$$

where S is the specific surface area,  $D_p$  is the size of the particles, and  $\rho$  is the density of particle [17,18].

#### Dislocation Density

The dislocation density is the length of dislocation lines per unit volume of the crystal [19]. A dislocation is a crystallographic deformity, or irregularity, within a crystal structure. The presence of dislocation will change the properties of materials. Scientifically, it is a kind of topological imperfection. It increases with plastic deformation; an instrument for the making of dislocations must be initiated in the material. Dislocation has three mechanisms which is homogeneous nucleation, grain boundary initiation, and interface, the lattice and the surface. It is well known that above a certain grain size limit (~30 nm). The material strength will increase with decreasing grain size [20,21]. The X-ray diffraction analysis has been used to evaluate the intrinsic stress and dislocation density [22,23]. The dislocation density ( $\delta$ ) in the sample has been determined using expressions.

$$\delta = \frac{1}{D^2}$$

where,  $\delta$ -dislocation density,  $\beta$ -diffraction broadening - measured at half of its maximum intensity (radian),  $\theta$ -diffraction angle (degree),  $\alpha$ - lattice constant (nm) and D-particle size (nm).

**Table 1.** Cell Parameters estimated from X-ray diffraction

D size nm	Dislocation density $\delta$	Morphology index x	surface area (nm) <sup>2</sup>	SSA m <sup>2</sup> g <sup>-1</sup>	SA to Vol Ratio
1.96E-08	2.593E+15	2.3094	1.211E-15	1.239E+15	5.237E+15
4.37E-06	5.226E+15	1.2500	6.012E-11	4.253E+19	1.795E+20
1.58E-08	3.991E+15	1.8050	7.836E-16	5.223E+14	2.302E+15
2.94E-08	1.157E+15	3.3444	2.712E-15	1.824E+15	7.775E+15
1.51E-08	4.405E+15	1.6583	7.142E-16	3.978E+14	1.657E+15
1.77E-08	3.182E+15	1.9047	9.815E-16	4.871E+14	2.063E+15
1.7E-08	3.481E+15	1.8115	9.228E-16	4.317E+14	1.849E+15
3.02E-08	1.096E+15	3.1152	2.577E-15	1.244E+15	5.245E+15
2.07E-08	2.328E+15	2.1326	1.924E-15	5.797E+14	2.452E+15
1.26E-08	2.779E+14	6.1369	1.986E-14	4.749E+15	2.023E+16
3.05E-08	1.077E+15	3.0303	2.605E-15	1.153E+15	4.889E+15

It is observed from the tabulated details and from Figure 5 dislocation density of the material is indirectly proportional to particle size. It implies that the

prepared TiO<sub>2</sub> nanoparticles have more strength and hardness than their bulk (TiO<sub>2</sub>) counterpart.

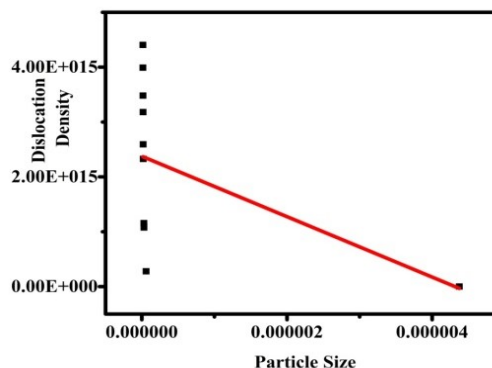


**Figure 5.** Particle Size Vs Dislocation Density of TiO<sub>2</sub> Nanoparticles

#### Morphology Index (MI)

The TiO<sub>2</sub> nanopowder is broadly utilized in many industries. Such uses are derived from its unique structural, physical and chemical properties, which are reflected by its surface properties, particle size, and morphology. The specific surface area of TiO<sub>2</sub> nanopowder depends on the interrelationships of particle size and morphology. MI is ascertained from FWHM of XRD, to investigate this relationship based on the literature reported [24].

MI is obtained using equation,

$$MI = \frac{FWHM_h}{FWHM_h + FWHM_p}$$

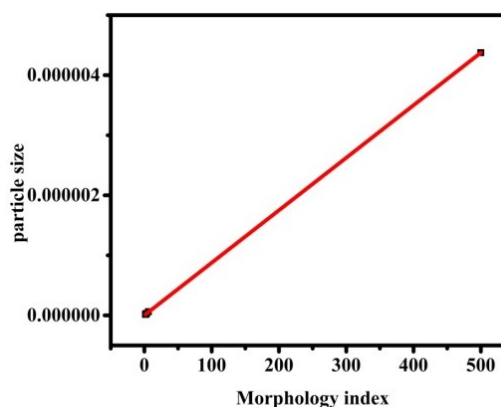


**Figure 6.** MI Vs Particle Size of TiO<sub>2</sub> Nanoparticles

where, MI is morphology index,  $FWHM_h$  highest FWHM value obtained from peaks and  $FWHM_p$  is particular peak's FWHM for which MI is to be calculated. MI range of experimental  $TiO_2$  nanopowder is from 1.8 to 6.1 and the details are presented in Table 1.

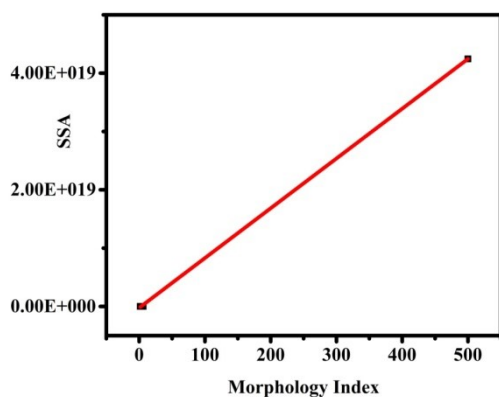


**Figure 7.** MI Vs Specific Surface Area of  $TiO_2$  Nanoparticles

It is correlated with the particle size (range from 15 to 45 nm) and specific surface area (range from 11.3 to 57.9  $m^2g^{-1}$ ). It is observed that MI is directly proportional to particle size and inversely proportional to the specific surface area with a small deviation. The results are shown in Figure 6 & 7. Linear fit in the figures demonstrates the deviations and relationships between them. The observed results of MI affirm the uniformity and fineness of the synthesized nanoparticles.

### Conclusion

$TiO_2$  nanoparticles were synthesized employing a flexible, non-toxic and bio-safe approach, at room temperature. This method is a single source, catalyst free, simple, conservative and environmentally benign which will make it suitable for various applications. XRD investigations have affirmed that the synthesized

particles are tetragonal anatase phase  $TiO_2$  and their nano size. The different characters like Instrumental broadening, specific surface area, dislocation density and morphology index were investigated by using XRD analysis.

### Acknowledgement

The authors are thankful to the University of Madras, Chennai for providing us the XRD instrumentation facilities to analyze the sample.

### References

- [1] M. Koelsch, S. Cassaignon, J.F. Guillemoles, J.P Jolivet, Comparison of optical and electrochemical properties of anatase and brookite  $TiO_2$  synthesized by the sol-gel method Thin Solid Film 403-404 (2002) 312-319.
- [2] H. Tang, K. Prasad, R. Sanjines, P.E. Schmid, and F.L & y Electrical and optical properties of  $TiO_2$  anatase thin films J. Appl. Phys. 75 (1994) 2042.
- [3] J.H. Braun, A. Baidins, R.E. Marganski,  $TiO_2$  pigment technology – review Prog. Org. Coat. 20 (1992) 105.
- [4] P.A. Mandelbaum, A.E. Reggazzoni, M.A. Blesa, Bilmes, S. A., The influence of applied bias potential on the photooxidation of methanol and salicylate on titanium dioxide films J. Phys. Chem. B 103 (1999) 5505.
- [5] J. Augustynski, J. Hinden, C. Stalder Novel Semiconducting Electrodes for the Photosensitized Electrolysis of Water, J. Electrochem. Soc.124 (1977) 1063.
- [6] P.S.M. Dunlop, J.A. Byrne, N. Manga, B.R. Eggs., The photocatalytic removal of bacterial pollutants from drinking water J. Photochem. Photobiol. 148 (2002) 355.

- [7] T. Ohzuku, T. Hirai, Nonaqueous An electrochromic displayed based on lithium/titanium dioxide cell. *Electrochim. Acta* 27 (1982) 1263.
- [8] K. J. Jiang, T. Kitamura, H. Yin, S. Ito and S. Yanagida, Dye-sensitized solar cells using brookite nanoparticle TiO<sub>2</sub> films as electrodes *Chem. Lett.*, 2002, 31(9), 872–873.
- [9] S.C. Tsai, Y.W. Chung, Effects of particle size on photoassisted water-gas shift reaction over Pt-TiO<sub>2</sub> *J. Catal.* 86 (1984) 231.
- [10] R. Krol, A. Goossens, J. Schoonman, Mott-Schottky Analysis of Nanometer-Scale Thin-Film Anatase TiO<sub>2</sub> *J. Electrochem. Soc.* 144 (1997) 1723.
- [11] C.J. Barbe', F. Arendse, P. Comte, M. Jirousek, F. Lenzmann., Nanocrystalline Titanium Oxide Electrodes for Photovoltaic Applications *J. Am. Ceram. Soc.* 80 (1997) 3157.
- [12] I. Cservednyak, G.H. Kelsall, W.Wang, Reduction of Ti-IV species in aqueous sulfuric and ... 1. titanium speciation *Electrochem. Acta* 23 (1997) 563.
- [13] Antic Z, Krsmanovic RM, Nikolic MG, Cincovic MM, Mitric M, Polizzi S, Dramicanin MD. Multisite luminescence of rare earth doped TiO<sub>2</sub> anatase nanoparticles. *Mat. Chem. Phys.* 135 (2012) 1064-1069.
- [14] Thamaphat K, Limsuwan P, Ngotawornchai B. Phase Characterization of TiO<sub>2</sub> Powder by XRD and TEM. *Kasetsart. J. (Nat. Sci.)* 42 (2008) 357-361.
- [15] S. Ito, P. Chen, P. Comte, M. Khaja, K. Nazeeruddin, P. Liska, P. Péchy and M.Grätzel, "Fabrication of Screen-Printing Pastes From TiO<sub>2</sub> Powders for Dye-Sensitized Solar Cells," *Progress in Photovoltaics: Research and Applications*, *Inter Science.* 56(2007) 465-472.
- [16] Ghosh SC, Thanachayanont C, Dutta J. Studies on Zinc sulphide nanoparticles for Field Emission Devices. The 1st ECTI Annual Conference (ECTI-CON 2004) Pattaya, Thailand 3-14 (2004) 145-148.
- [17] Jiji A, Joseph N, Donald RB, Daniel M, Amit S, You Qiang. Size-Dependent Specific Surface Area of Nanoporous Film Assembled by Core-Shell Iron Nanocluster. *J. Nanomater.* 54961 (2006) 1-4.
- [18] L, Ki-Won J, Jin-OokBg, Dae JY. Chemical Synthesis and Characterization of Highly Oil Dispersed MgO Nanoparticles. *J.Ind. Eng. Chem.* 12(6) (2006) 882-887.
- [19] Nehru LC, Swaminathan V, Sanjeeviraja C. Photoluminescence Studies on Nanocrystalline Tin Oxide Powder for Optoelectronic Devices *American. J. Mat. Sci.* 2(2) (2012) 6-10.
- [20] Gubicza J, Chinh NQ, Lábár JL, Z. Heged Delayed microstructural recovery in silver processed by equal-channel angular pressing. *J Mater Sci.* 43 (2008) 5672–5676.
- [21] Majeed Khan MA, Kumar S, Ahamed M, Alrokayan SA, Alsalhi MS. Structural and thermal studies of silver nanoparticles and electrical transport study of their thin films. *Nanoscale.Res.Lett.* 6 (2011) 434.
- [22] Subbaiah YPV, Prathap P, Reddy KTR. Structural, electrical and optical properties of ZnS films deposited by close-spaced evaporation. *Appl. Surf. Sci.* 253(5) (2006) 2409-2415.
- [23] Velumani S, Mathew X, Sebastian PJ, Narayandass Sa K, Mangalaraj D. Structural and optical properties of hot wall deposited CdSe thin films. *Solar Energy Material & Solar Cells.* 76(3) (2003) 347-358.
- [24] Theivasanthi T, Alagar M, An Insight Analysis of Nano sized powder of Jackfruit Seed. *Nano Biomed Eng.* 3 (2011)163–168.